



**Manchester  
Metropolitan  
University**

---

Oien, Rachel and Spagnolo, Matteo and Rea, Brice and Barr, Iestyn and Bingham, Robert (2019) Climatic controls on the equilibrium-line altitudes of Scandinavian cirque glaciers. *Geomorphology*. ISSN 0169-555X

---

**Downloaded from:** <http://e-space.mmu.ac.uk/624552/>

**Version:** Accepted Version

**Publisher:** Elsevier

**DOI:** <https://doi.org/10.1016/j.geomorph.2019.106986>

**Usage rights:** Creative Commons: Attribution-Noncommercial-No Derivative Works 4.0

Please cite the published version

<https://e-space.mmu.ac.uk>

1 **Climatic controls on the equilibrium-line altitudes of Scandinavian cirque glaciers**

2

3 Rachel P. Oien<sup>1</sup> (r.oien@abdn.ac.uk)\*, Matteo Spagnolo<sup>1</sup> (m.spagnolo@abdn.ac.uk), Brice R. Rea<sup>1</sup>

4 (b.rea@abdn.ac.uk), Iestyn D. Barr<sup>2</sup> (I.Barr@mmu.ac.uk), and Robert G. Bingham<sup>3</sup>

5 (r.bingham@ed.ac.uk)

6 \*corresponding author

7 <sup>1</sup> University of Aberdeen, School of Geosciences, Department of Geography & Environment, St.

8 Mary's Building, Elphinstone Road, Aberdeen, United Kingdom AB24 3TU

9 <sup>2</sup> Manchester Metropolitan University, Department of Natural Sciences, Manchester, United Kingdom

10 M1 5GD

11 <sup>3</sup> University of Edinburgh, School of GeoSciences, Drummond Street, Edinburgh, United Kingdom

12 EH8 9XP

13

14 Keywords: equilibrium-line altitude (ELA), Scandinavian cirque glaciers, precipitation, temperature,

15 GIS

16

17

18 **Abstract**

19 The equilibrium-line altitudes (ELAs) of reconstructed palaeoglaciers have been widely used

20 to assess palaeoclimatic conditions, yet this concept has rarely been tested using modern glaciers. To

21 address this shortcoming, correlations between the ELAs of 513 modern cirque glaciers and present-

22 day climatic and topographic variables across Scandinavia, as well as regional trends in ELA and

23 climate, are analysed. ELAs are calculated using the Area-Altitude-Balance-Ratio method, with a

24 ratio of  $1.5 \pm 0.4$ . Results indicate that glacier ELAs are strongly correlated with distance from the

25 coast. This reflects the present-day precipitation pattern of the region (characterised by high

26 precipitation near the sea) and demonstrates a climate dominated by a maritime-continental transition.

27 Temperature explains differences in glacier ELA regional trends as well as ELA changes with

28 latitude. Following standard meteorological convention, Scandinavia is divided into two macro-

29 climate regions and analyses are run within the macro-regions as well as the complete dataset. The  
30 strength of correlations between ELA and precipitation increases when the study is divided into  
31 northern and southern macro-regions. These results test long held assumptions about relationships  
32 between climate and cirque glacier ELA, which is of particular relevance to palaeoclimatic studies  
33 based on the reconstruction of former cirque glaciers.

34

## 35 **1.0 Introduction**

36 Glacier mass balance can be approximated by a single parameter, an equilibrium-line altitude  
37 (ELA), which reflects the annual balance between accumulation and ablation (Sutherland, 1984;  
38 Ohmura et al., 1992; Benn et al., 2000). Accumulation inputs are precipitation (solid and liquid),  
39 avalanching and windblown snow. The accumulation zone is the area of positive mass balance at the  
40 end of the mass balance year (typically September in the Northern Hemisphere). Ablation, the process  
41 of mass loss, occurs through surface melting, sublimation and, where applicable, submarine melting  
42 and iceberg calving. The ablation zone is the area of negative mass balance at the end of the mass  
43 balance year. The ELA is the elevation that divides these two zones (i.e., the position of zero annual  
44 net mass balance), and is largely determined by local climate (esp. ablation season air temperature and  
45 accumulation season precipitation), which exerts a fundamental control on mass balance (Oerlemans  
46 and Hoogendoorn, 1989; Ohmura et al., 1992; Benn et al., 2000; Winkler et al., 2009; Rea, 2009;  
47 Ohmura and Boettcher, 2018). Perturbations of either one of the two climate variables will impact  
48 glacier mass balance and ELA, resulting in either glacier advance or retreat. Due to this relationship,  
49 ELAs, or trends therein, can be used as a proxy for climate and/or climate gradients. This is of  
50 particular relevance in formerly glaciated regions, where reconstructed ELAs (derived through  
51 various methods) are assumed to provide a palaeoclimate proxy (Torsnes et al., 1993; Benn et al.,  
52 2000; Carrivick and Brewer, 2004; Barr and Spagnolo, 2015a). For example, cirque floor elevation,  
53 which is considered a proxy for cirque glacier ELA, has been used to reconstruct regional palaeo-  
54 precipitation and temperature trends (Barr and Spagnolo, 2015b; Barr et al., 2017). However,  
55 relatively few studies have conducted a rigorous test of the validity of using ELA trends as a proxy for

56 climate gradients, based on modern glaciers and climate (Rupper and Roe, 2008; Sagredo et al.,  
57 2014). Mostly, this is due to a lack of measured (i.e. calculated from long term mass balance field  
58 data) ELAs. Recent developments in the availability of high-resolution digital elevation models  
59 (DEMs), GIS tools, global inventories of mapped glacier outlines, and global climate data can now be  
60 exploited to fill this gap (Braithwaite and Raper, 2009). In this study, we utilise such datasets to  
61 investigate relationships between the ELAs of modern cirque glaciers and present-day climate across  
62 Norway and Sweden.

63

## 64 **2.0 Methods**

### 65 **2.1 Selecting glaciers**

66 Cirque glaciers are abundant, simple in their morphology, and relatively small, therefore they  
67 have a short response time and are sensitive to climate forcing (Trenhaile, 1975; Rosqvist and Østrem,  
68 1989; Grudd, 1990; Rudberg, 1994; Fujita, 2008; Winkler et al., 2009). This paper considers only  
69 cirque glaciers, i.e. larger ice masses, ice caps, plateau and valley glaciers, were not included.  
70 Polygons delineating the perimeters of all of Scandinavia's ~1600 modern glaciers were obtained  
71 from the Norwegian Water Resources and Energy Directorate (NVE). These glaciers were mapped  
72 from Landsat TM/ETM+ satellite imagery, acquired between 1999 and 2006 (Andreassen et al., 2012;  
73 Winsvold et al., 2014), and are part of the GLIMS global glacier database (GLIMS and NSIDC, 2005,  
74 updated 2018; Raup et al., 2007). For this study, each glacier was labelled using its unique GLIMS  
75 code. Cirque glaciers (n = 513) were identified using the definition by Evans and Cox (1974) and  
76 contoured at 15 m intervals using a 10 m resolution DEM (Norwegian Mapping Authority, 2016,  
77 Figure 1). We also used Google Earth imagery from the 2006 ablation season to confirm the presence  
78 of all cirque glaciers (Figure 2).

### 79 **2.2 Calculating ELAs**

80 The most accurate way to determine the ELA of a modern glacier is directly from its mass  
81 balance, ideally measured for at least 10 consecutive years (Rea, 2009). However, worldwide there

82 are <150 glaciers which have at least 10 years of continuous direct mass-balance measurements  
83 (Braithwaite, 2009), none of which are cirque glaciers in Scandinavia. An alternative approach is to  
84 derive the ELA from glacier geometry (Trenhaile, 1975; Rosqvist and Østrem, 1989; Grudd, 1990;  
85 Nesje, 1992; Torsnes et al., 1993; Osmaston, 2005). We adopt the latter approach, using a GIS tool  
86 developed by Pellitero et al. (2015) which only requires a DEM and mapped polygons of glacier  
87 perimeters as inputs. While there are different techniques to calculate a glacier ELA (Pellitero et al.,  
88 2015), the ELA of the modern 513 Scandinavian cirque glaciers were calculated using the Area  
89 Altitude Balance Ratio (AABR) and Accumulation Area Ratio (AAR) methods only, following Rea  
90 (2009). Ratios of  $1.5 \pm 0.4$  and 0.58 were selected for the AABR and AAR, respectively, based on the  
91 regional values obtained from the analysis of measured ELAs in Scandinavia (Rea, 2009). For the 513  
92 cirque glaciers, the difference between ELAs calculated using the AABR and AAR methods is less  
93 than 5 m. Henceforth, for the sake of simplicity, the only ELAs discussed in this paper are those  
94 derived using the AABR method.

### 95 **2.3 ELA validation**

96 While our study focuses on cirque glaciers in Scandinavia, in order to validate this approach,  
97 we compared GIS-calculated (using the AABR and AAR methods) and measured ELAs for 11  
98 Scandinavian valley and plateau glaciers. These are the only Scandinavian glaciers ELAs from the  
99 World Glacier Monitoring Service (WGMS) that have been derived from measured mass balance  
100 records spanning at least 10 years, including the 1999-2006 period, which corresponds to the  
101 timeframe of the cirque glacier mapping (Winsvold et al., 2014; Kjøllemann, 2017). For each glacier,  
102 the zero net mass balance was calculated by plotting the annual specific net balance versus the ELA,  
103 following Rea (2009). The GIS-calculated and measured ELAs are highly correlated ( $r^2 = 0.99$ ). The  
104 average difference between the GIS-calculated and zero net mass balance measured ELAs is 26.2 m,  
105 which is minimal given other uncertainties in mass balance measurements. This indicates that the  
106 GIS-calculated ELAs represent good estimates of measured ELAs and are reliable for the analysis of  
107 regional trends.

108

### 109 **2.4 Comparison with climate**

110 To compare ELAs with climate, we extracted a series of climatic parameters at the ELA of  
111 the 513 cirque glaciers and analysed their regional trends. We obtained gridded (1 km x 1 km)  
112 precipitation and temperature data from the NVE for the period 1976 to 2006 (<http://seNorge.no>;  
113 Engelhardt et al., 2012; Lussana et al., 2016; Wong et al., 2016). This period was chosen because the  
114 glacier outlines were mapped between 1999 and 2006, and we assume their geometry is a function of  
115 the climate averaged over the previous 30 years (Andreassen et al., 2012). For temperature, grids of  
116 mean summer (JJA) air temperature (Figure 3) and mean annual air temperature (MAAT) were  
117 generated. For precipitation, grids of mean winter (DJF) precipitation (Figure 4) and mean annual  
118 precipitation were generated. Glacier latitude, aspect, solar radiation and distance from the coast were  
119 also considered, since these parameters have previously been suggested, or are known, to have an  
120 influence on cirque glacier ELAs (Sutherland, 1984; Rosqvist and Østrem, 1989; Evans, 2006a; Raper  
121 and Braithwaite, 2009; Křížek and Mida, 2013; Barr and Spagnolo, 2015a). Aspect was calculated  
122 using the ACME ArcGIS tool (Spagnolo et al., 2017). Solar radiation was calculated using the ‘area  
123 solar radiation’ ArcGIS tool, and a mean value was calculated for each glacier. The coast was defined  
124 as a manually digitised line that excluded fjords, and the Euclidian distance from each glacier to this  
125 line was measured using the ‘Near’ ArcGIS tool. A midpoint was placed along the ELA contour of  
126 each cirque glacier and used to extract temperature, precipitation, and latitude from the relevant  
127 gridded datasets.

128 Climatically, the study region can be divided into two macro-regions: a southern ‘temperate’,  
129 macro-region, influenced by the North Atlantic Current; and a northern ‘polar/subpolar’ macro-  
130 region, proximal to the polar front and Siberia (Tveito et al., 2000). The cirque glacier database can  
131 also be divided into northern and southern macro-regions, separated by a major topographic saddle in  
132 the Scandinavian mountains. This division, at ~64°N (Figure 1), corresponds approximately to the  
133 climatic divide, north of which there are 255 cirque glaciers and south of which there are 258. Given  
134 this natural division, analyses were conducted on the entire cirque glacier dataset as well as separately  
135 on the two macro-regions. Notably, within the southern macro-region, there is a strong west-east  
136 gradient, from a maritime to continental climate. This gradient, while discussed in the Scandinavian  
137 glacier literature (e.g. Torsnes, 1993; Nesje et al., 2008; Nesje, 2009; Winkler et al., 2009; Winsvold

138 et al., 2014), does not have a distinct boundary which defines the transition, and therefore the dataset  
139 was not subdivided further or defined as its own macro- region. Further climatic subregions might  
140 exist and certainly existed in the past, however, these are not considered in the present work, which  
141 focuses on how present-day climatic trends are reflected in modern cirque glacier ELAs.

142 Plots showing regional trends in ELA, elevation, winter precipitation and summer  
143 temperature (the two climatic parameters known to affect glacier mass balance the most) were also  
144 generated (Figure 7), showing how these variables change with distance from the coast. In order to  
145 investigate the regional climates, 10 km-wide swaths parallel to the coastline were constructed.  
146 ArcGIS zonal statistics were used to extract minimum, mean and maximum values for each parameter  
147 (ELA, elevation, winter precipitation and summer temperature) within each swath. Neither  
148 temperature nor precipitation were reduced to sea level, as it is the value at the elevation of the  
149 glaciers that matters when it comes to identifying how mass balance and ELA respond to climate. The  
150 northern macro-region contains cirque glaciers from 0 km to 150 km from the coast, while the  
151 southern macro-region contains cirque glaciers between 30 km and 200 km from the coast. To allow  
152 comparison between the two macro-regions, climate and ELA trends were analysed between 30 km  
153 and 150 km from the modern coast.

154 We use the above data to analyse correlations between ELA and all possible controls, then  
155 apply Principal Component Analysis (PCA) to explore these relationships further.

156

## 157 **3.0 Results**

### 158 **3.1 ELA analysis for the entire dataset**

159 The 513 cirque glaciers analysed in this study cover 200 km of longitude and 1400 km of  
160 latitude (Figure 1). The calculated ELAs for these glaciers range from 495 m to 2027 m. The lowest  
161 ELAs are found near the coast, primarily in the north, and the highest ELAs are found inland in the  
162 south (Figure 3). Taking the dataset as a whole, Pearson correlations between glacier ELA and the  
163 other parameters, which have been extracted at the ELA, range from -0.828 to +0.817 (Table 1). The  
164 strongest correlation ( $r = -0.828$ ) is between ELA and mean summer air temperature, and the second

165 strongest is with distance from the coast ( $r = 0.817$ ) (Table 1). Latitude and MAAT also have strong  
166 negative correlations with ELA. Solar radiation is positively, but weakly, correlated with ELA;  
167 precipitation is negatively, but weakly, correlated with ELA ( $r = -0.187$  for annual, and  $-0.249$  for  
168 winter).

### 169 **3.2 Principal Component Analysis**

170 Using the above data, PCA (Figure 5) supports the finding that distance from the coast and  
171 ELA co-vary, as demonstrated by the acuteness of the angle between the two variables. Another  
172 important relationship identified from this analysis is that the southern macro-region can be further  
173 subdivided into two groups. One of the principal components is distance from the coast, while the  
174 other is precipitation, both winter and annual (Figure 5). The PCA of the northern cirque glaciers  
175 primarily clusters around the axes of MAAT and mean summer air temperature.

### 176 **3.3 Macro-region ELA analysis**

177 The strength of the correlation between ELA and air temperature, both MAAT and mean  
178 summer, changes little when analysed at the macro-region level. Negative correlations between ELA  
179 and MAAT are very strong in both the northern and southern regions (Table 1). Negative correlations  
180 between ELA and mean summer air temperature are strong in the northern region and very strong in  
181 the southern region (Table 1). Correlations between precipitation and ELA are weak in the northern  
182 region ( $r = +0.118$  and  $+0.105$  for annual and winter totals, respectively) but very strong in the  
183 southern region ( $r = -0.783$  and  $-0.790$  for annual and winter totals, respectively). The strength of the  
184 correlations between ELA and distance from the coast remains comparable to the full dataset in both  
185 the northern and southern regions, as do correlations with aspect and solar radiation. The negative  
186 correlation between ELA and latitude remains strong in the northern region ( $r = -0.505$ ), while it  
187 weakens in the southern region ( $r = -0.165$ ).

### 188 **3.4 The role of continentality**

189 The entire dataset shows a strong negative correlation between distance from the coast and  
190 temperature, both MAAT and mean summer. At the macro-regional scale, the correlation between



191 distance from the coast and MAAT, in both the northern and southern regions, becomes very strongly  
192 negative (Table 2). The negative correlation between distance from the coast and mean summer  
193 temperature weakens in the northern region ( $r = -0.431$ ) yet remains strong in the southern region ( $r =$   
194  $-0.643$ ). Distance from the coast and precipitation are weakly negatively correlated for the whole  
195 dataset ( $r = -0.266$  and  $-0.311$ , for annual and winter precipitation, respectively). In the northern  
196 region, this relationship remains weakly negative ( $r = -0.142$  and  $-0.107$  for annual and winter  
197 precipitation, respectively), but is strongly negative in the southern region ( $r = -0.558$  and  $-0.582$  for  
198 annual and winter precipitation, respectively).

### 199 **3.5 Climate trends across Scandinavia**

200 Climate trends in Scandinavia are affected by the presence of the mountain range that extends  
201 the length of Norway. The altitudinal effect of topography is reflected in the mass balance of the  
202 region's glaciers. Using the buffer zones, regional climatic patterns (not climate at the ELA) could be  
203 evaluated using swaths as distance from the coast (Figure 6). With distance from the coast,  
204 temperature and precipitation generally decrease, while ELA increases, in both the southern and  
205 northern regions.

206 In the northern region, summer temperature declines inland with a gradient of  $-0.09^{\circ}\text{C}/10\text{ km}$   
207 and the lowest average summer temperature of  $8.76^{\circ}\text{C}$  occurs within the interval 110-120 km from the  
208 coast. In the southern region, average summer temperature declines inland with a gradient of  $-$   
209  $0.25^{\circ}\text{C}/10\text{ km}$ , reaching its lowest value of  $8.2^{\circ}\text{C}$  at 115 km inland, which is the highest topography in  
210 the southern Scandinavian Mountains, near Jotunheimen. The lowest average summer temperature in  
211 the southern region is  $8.22^{\circ}\text{C}$ , 100-110 km from the coast. In the northern region, winter precipitation  
212 decreases inland with a gradient of  $-12.9\text{ mm}/10\text{ km}$ , and a minimum value of 427.4 mm occurs  $\sim$ 105  
213 km from the coast. In the southern region, winter precipitation decreases inland with a gradient of  $-$   
214  $39.3\text{ mm}/10\text{ km}$ , and a minimum value of 166.8 mm occurs  $\sim$ 205 km from the coast. The mean  
215 elevation of topography generally increases inland with a gradient of  $39.2\text{ m}/10\text{ km}$  in the northern  
216 region and  $61.0\text{ m}/10\text{ km}$  in the southern region. Glacier ELAs show similar patterns, i.e. ELAs  
217 increase inland at  $44.5\text{ m}/10\text{ km}$  and  $59.0\text{ m}/10\text{ km}$ , in the northern and southern regions, respectively.

218

## 219 **4.0 Discussion**

### 220 **4.1 Controls on cirque glacier ELAs**

221 Our findings suggest that multiple, sometimes competing, factors influence modern cirque  
222 glacier ELAs across Scandinavia. The strong correlation of ELA with distance from the coast likely  
223 reflects the competing role of present-day temperature (Figure 3) and precipitation (Figure 4) on  
224 glacier mass balance. Both temperature and precipitation decline with distance inland, which would  
225 have opposite effects on ELA. The strong rise in ELA with distance inland implies that reduced  
226 precipitation exerts the stronger influence, but temperature still plays a role, as demonstrated by the  
227 analyses of the two macro-regions (Figure 6). In the south, summer temperature decreases inland at a  
228 relatively high rate, mainly caused by rising elevation (Figure 6b). Despite the general decrease in  
229 summer temperature inland that would tend to lower the ELA, the ELA increases inland because of  
230 the very strong declining precipitation gradient in the southern Scandinavian mountains (Figure 6d),  
231 as also noted by others in this same region (Winkler and Nesje, 2009; Winkler et al., 2009; Trachsel  
232 and Nesje, 2015). In the north, the winter precipitation gradient inland is much weaker (Figure 6c) but  
233 so is the summer temperature gradient (Figure 6a), and the combined effect of the two on glacier mass  
234 balance means that the ELA increases inland here, as it did in the south. This general finding mirrors  
235 that of Sagredo et al. (2014), who analysed ELA/climate relationships in the Andes. The strong link  
236 between precipitation gradients and ELA suggests that continentality, and specifically moisture  
237 availability, is a key control on ELA within the Scandinavian mountains. Disparity between  
238 continental and maritime climates has long been hypothesised to exert the strongest climatic impact  
239 on glacier mass balance globally (Braithwaite, 1984).

240 While precipitation is the key parameter in determining how glacier ELA changes with  
241 distance to the coast, temperature becomes the dominant influence on latitudinal ELA trends. This is  
242 demonstrated by the negative correlation between ELA and latitude (Table 1). The larger latitudinal  
243 range of the northern region ( $5.5^\circ$ ) relative to that of the southern region ( $3^\circ$ ) contributes to the

244 stronger ELA/latitude correlation in northern Scandinavia (Table 1). The effect of temperature could  
245 also be seen in the distribution of cirque glaciers, which is very different between the two macro-  
246 regions. More glaciers are found close to the coast in the north than in the south (16.6% vs. 1.2%,  
247 within the first 50 km), most likely reflecting the fact that temperatures near the coast are lower in the  
248 northern region (Figure 6a).

249         Several previous studies have highlighted the influence of aspect on cirque glaciation. For  
250 example, Evans (2006b; 2011) has demonstrated that in the northern hemisphere, and more  
251 specifically in Scandinavia, cirques favour formation in NE aspects. Here, winter accumulation could  
252 be accentuated through windblown deposition and melting is suppressed by reduced exposure to solar  
253 radiation over diurnal cycles, with the maximum sunlight occurring in the mornings when  
254 temperatures are cooler (Chueca and Julián, 2004; Barr and Spagnolo, 2015a). Most of the analysed  
255 cirque glaciers are characterised by a NE aspect with a vector mean of 41° (Figure 7). The weak  
256 correlation between cirque glacier received solar radiation and ELA, suggests that rather than  
257 controlling present-day cirque glacier ELAs, aspect and solar radiation affect sites of glacier  
258 initiation—thereby controlling where modern cirque glaciers are located.

259         Although some of the relationships explored imply that climatic factors strongly influence  
260 cirque glacier ELA, a further possibility is that there is a significant direct topographic control, in that  
261 high- and low-altitude cirque glaciers can only form where high- and low-altitude topography exist.  
262 The distribution of glaciers relative to elevation is an aspect of great relevance for regional studies on  
263 glacier ELA because it demonstrates that non-climatic variables, such as topographic availability,  
264 might affect cirque glacier distributions. Specifically, climate might determine a theoretical ELA that  
265 is higher than the available elevation in a landscape, but glaciers can only be present where there is a  
266 landscape on which to form. Within our study, only 19% of the glaciers occur at an elevation that is  
267 more than 300 m below the highest surrounding (within 2 km) topography. Regional ELA trends may,  
268 in some cases, be limited by topographic availability rather than representing a direct proxy for  
269 climate (Anders et al., 2010).

## 270         **4.2 Implications for palaeoclimate reconstruction**

271 For the purpose of palaeoenvironmental reconstruction, it is often assumed that former cirque  
272 glacier ELAs are proxies for palaeoclimate (Evans, 2006b; Pearce et al., 2017; Ipsen et al., 2018).  
273 This applies to ELAs calculated from three-dimensional palaeoglacier reconstructions, and to more  
274 simple estimates of ELAs, for example from cirque-floor altitudes (Benn et al., 2000; Barr and  
275 Spagnolo, 2015a). This has also been applied to palaeoenvironmental studies where distance from the  
276 coast has been used as a proxy for palaeoprecipitation and linked to changes in palaeoglacier ELAs  
277 (Barr and Spagnolo, 2015b).

278 Results from this study, which focuses on modern cirque glaciers and present-day climate,  
279 support the idea that cirque ELA is controlled by climate, and is therefore, a valid palaeoclimatic  
280 proxy, but with a few caveats. For example, our study has demonstrated clear regional (northern vs.  
281 southern Scandinavia) differences in controls on ELA. Importantly, there are a number of parameters  
282 where the strength of correlation changes considerably depending on the size of the study area. For  
283 example, the correlation between precipitation, especially winter, and ELA changes from very weak,  
284 for the whole dataset, to very strong, for the southern region. The geographical split of the dataset into  
285 two regions was dictated by knowledge of present-day Scandinavia climate, characterised by the  
286 presence of two major climatic zones ('polar/subpolar' in the north and 'temperate' in the south)  
287 (Tveito et al., 2000). The North Atlantic Oscillation controls a large amount of winter precipitation  
288 throughout Scandinavia (Hanssen-Bauer, 2005). The North Atlantic Current, which extends to the  
289 Norwegian Current, creates a milder climate than expected at such high latitudes. The climatic  
290 distinction between these two zones was further confirmed by the PCA which clearly identifies the  
291 two regions based on a primary climate variable and subgroups within those regions. However, all this  
292 information was only available to us because we were dealing with present-day climate. In a  
293 palaeoclimate context, splitting glacier populations on the basis of assumed palaeoclimate differences  
294 is non-trivial, and possibly circular, since the aim of such studies is often to use palaeoglacier ELAs to  
295 reconstruct former climate. Therefore, one recommendation from this study is that in order to interpret  
296 palaeo ELA trends, datasets covering large regions, with the potential to extend over multiple climatic  
297 zones, should be sub-divided in multiple ways, to highlight potential sub-populations (i.e. ELA

298 gradients should be analysed on a regional basis) (Evans, 2006a; Barr and Spagnolo, 2015a). In the  
299 first instance this sub-division should be guided by obvious physiographic characteristics. Additional  
300 information regarding past climate, which could be extracted from other proxies such as tree rings,  
301 speleothems (cave deposits) and lacustrine and marine deposits which contain foraminifera, pollen,  
302 diatoms, microfossils and chironomids (e.g. Kellogg, 1977; Mangerud et al., 1981; Lauritzen, 1995;  
303 Hertzberg and Schmidt, 2006; Baker, 2009; Skoglund and Lauritzen, 2010; Bakke et al., 2013; Olsen  
304 et al., 2013; Jansen et al., 2016), could also prove useful in guiding a regional analysis. However,  
305 caution should be applied when using other proxies to define regional climates to ensure they do not  
306 compromise subsequent palaeoprecipitation calculations derived from the ELAs i.e. circularity should  
307 be avoided.

308         The present study focuses on cirque glacier ELAs at a fixed point in time (i.e. the present),  
309 however, studies which use cirque-floor altitudes as a proxy for palaeoclimate often ignore the time  
310 transgressive nature of their occupation. In Figure 7, there is a swath of topography which is currently  
311 occupied by cirque glaciers, from a minimum elevation generally to the highest elevation at which  
312 topography allows a cirque to exist. There are in many instances un-occupied cirques below the  
313 present-day minimum elevation, because temperature is too high. As climate changes this lower limit  
314 to glaciation migrates most likely in response to temperature, unless there is a major change in  
315 precipitation. When climate is warmer the cirque-occupation swath becomes increasingly limited by  
316 topographic availability. Conversely as climate cools the minimum elevation for cirque-occupation  
317 lowers and the swath elevation range increases with, at some point, higher elevation cirque glaciers  
318 expanding and coalescing to form valley glaciers. When assessing a deglaciated landscape, using  
319 cirques as a paleoclimate proxy, all cirques are grouped, ignoring the time transgressive nature of their  
320 occupation. Further work is required to assess how best to interpret the paleoclimate signal from a  
321 landscape-scale analysis of cirques, but the gradient in minimum cirque elevation is most likely to  
322 represent a temporally coherent dataset.

323

## 324 **5.0 Conclusions**

325 We used ArcGIS, high-resolution mapping and present-day climate to assess the relationships  
326 between modern cirque glacier ELAs and climate, with a focus on Scandinavia. The most significant  
327 findings are:

- 328 • One of the strongest relationships is between ELA and distance from the coast, with  
329 ELA increasing inland. This reflects the strong maritime-continental transition that  
330 characterises the region. The correlation between the two parameters most likely  
331 results from a relatively strong precipitation gradient coupled with a weak  
332 temperature gradient in the south, and a weaker precipitation gradient coupled with a  
333 weaker temperature gradient in the north. This illustrates the competing effect of  
334 temperature and precipitation on glacier ELA.
- 335 • The strength of a number of correlations between modern glacier ELA and present-  
336 day climatic and topographic parameters changes depending on the extent of the  
337 study area (Scandinavia versus two smaller macro-regions). This highlights the  
338 importance of regional climate variability in controlling ELA trends and it is of  
339 particular relevance to palaeoglacier reconstructions because the data with which to  
340 define regional differences will be limited and may be the target of the glacier  
341 reconstructions. Bigger is not necessarily better and it is recommended that large  
342 datasets also be analysed as subsets, defined by physiographic and/or other  
343 paleoclimate proxies. Caution should be applied to avoid circularity if  
344 palaeoprecipitation is to be calculated.
- 345 • If assessing a landscape of un-occupied cirques for paleoclimate interpretation, care  
346 must be taken to consider the time transgressive nature of cirque occupation. The  
347 gradient in minimum cirque elevation is most likely to represent a temporally  
348 coherent dataset.
- 349 • Topographic availability matters: if there is no topography at the theoretical ELA,  
350 glaciers cannot form, and this might affect apparent ELA-climatic gradients.

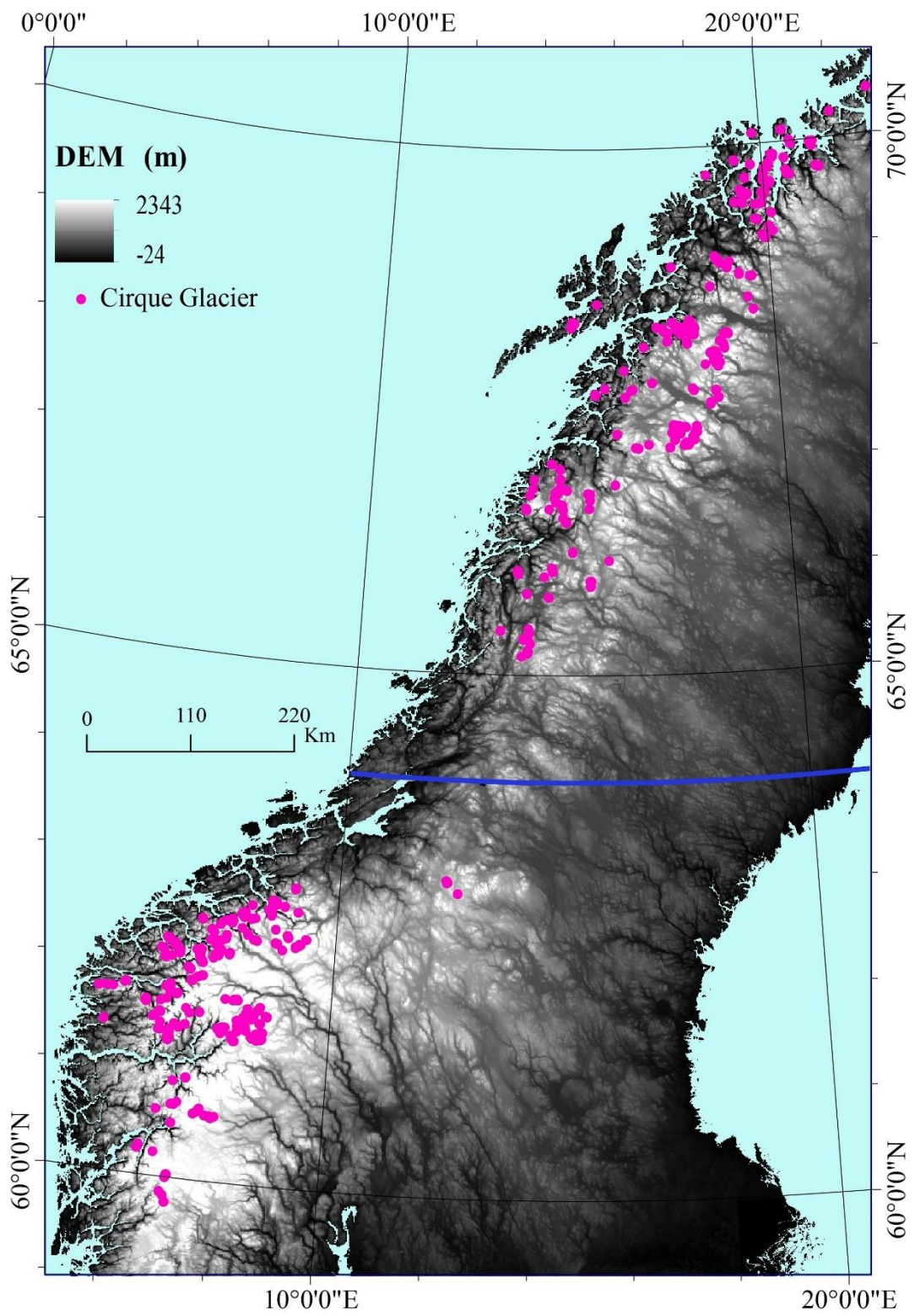
351

352 **6.0 Acknowledgements**

353 Dr. Dmitri Mauquoy is acknowledged for his help with the statistical analyses. We would like to  
354 thank the Scottish Alliance for Geoscience, Environment and Society for the funding RO's PhD  
355 scholarship and continual contributions towards travel and training. We would also like to extend  
356 thanks to The North Theme, at the University Aberdeen for support to attend a summer school in  
357 palaeoclimatology. Two anonymous reviewers and the Editor are acknowledged for their constructive  
358 and insightful comments.

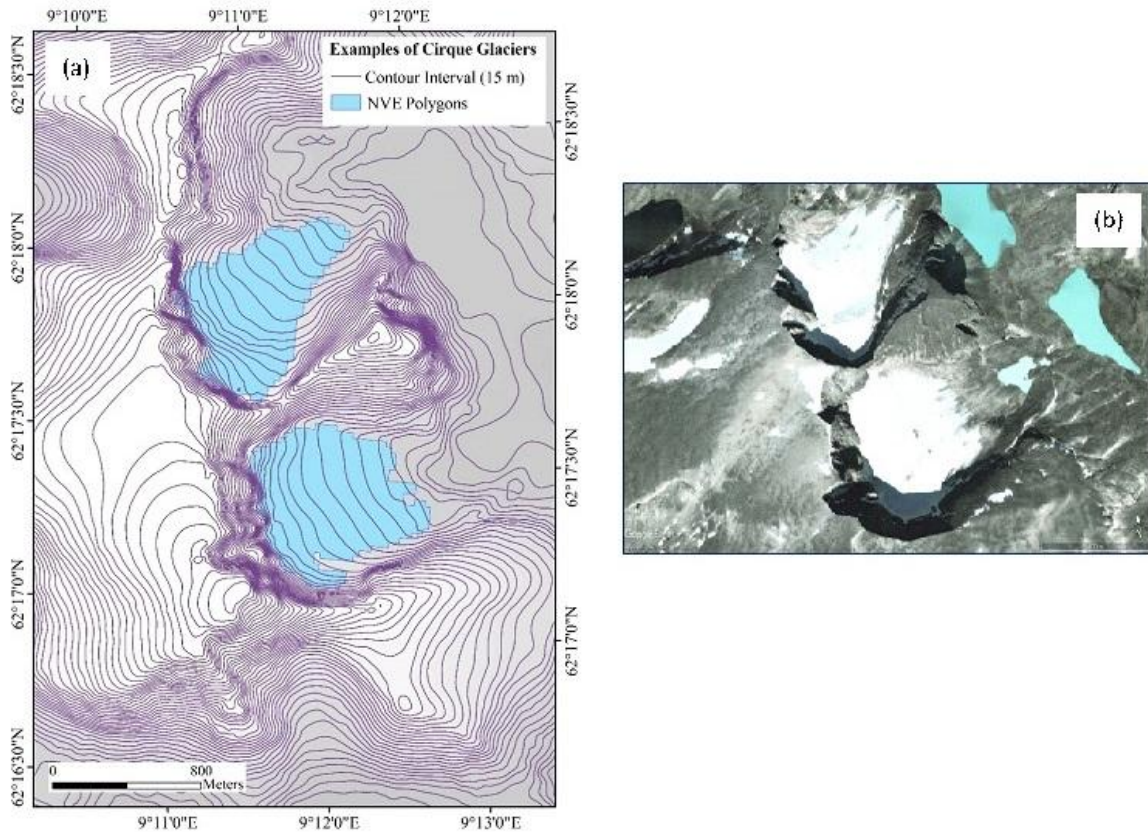
359

360 **7.0 Figures**

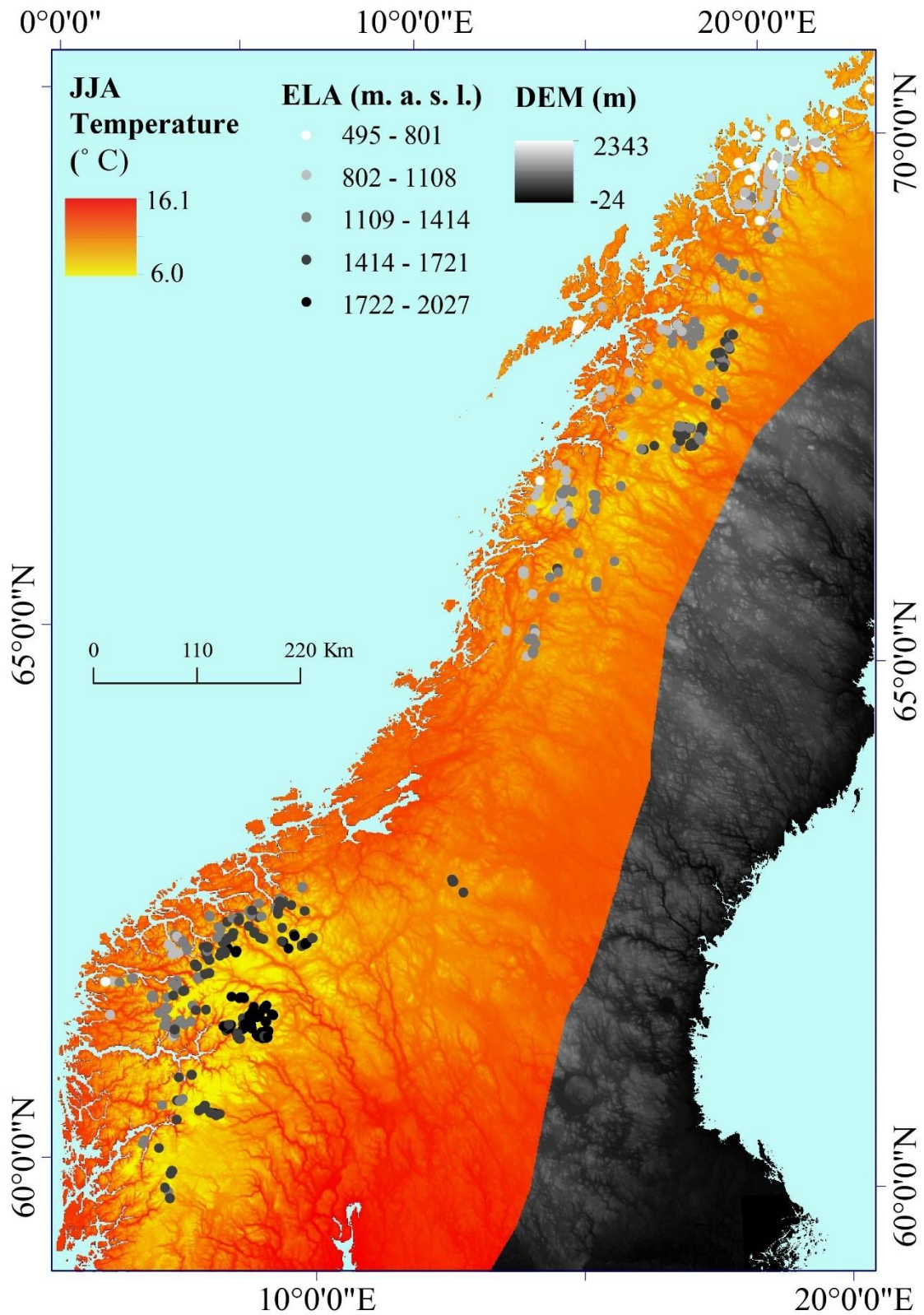




362 Figure 1: Locations of cirque glaciers analysed within this study (pink dots). The topographic saddle  
363 at  $\sim 64^\circ\text{N}$  coincides with a latitudinal change in climatic zones. The thick blue line separates the two  
364 macro-regions discussed in the text.

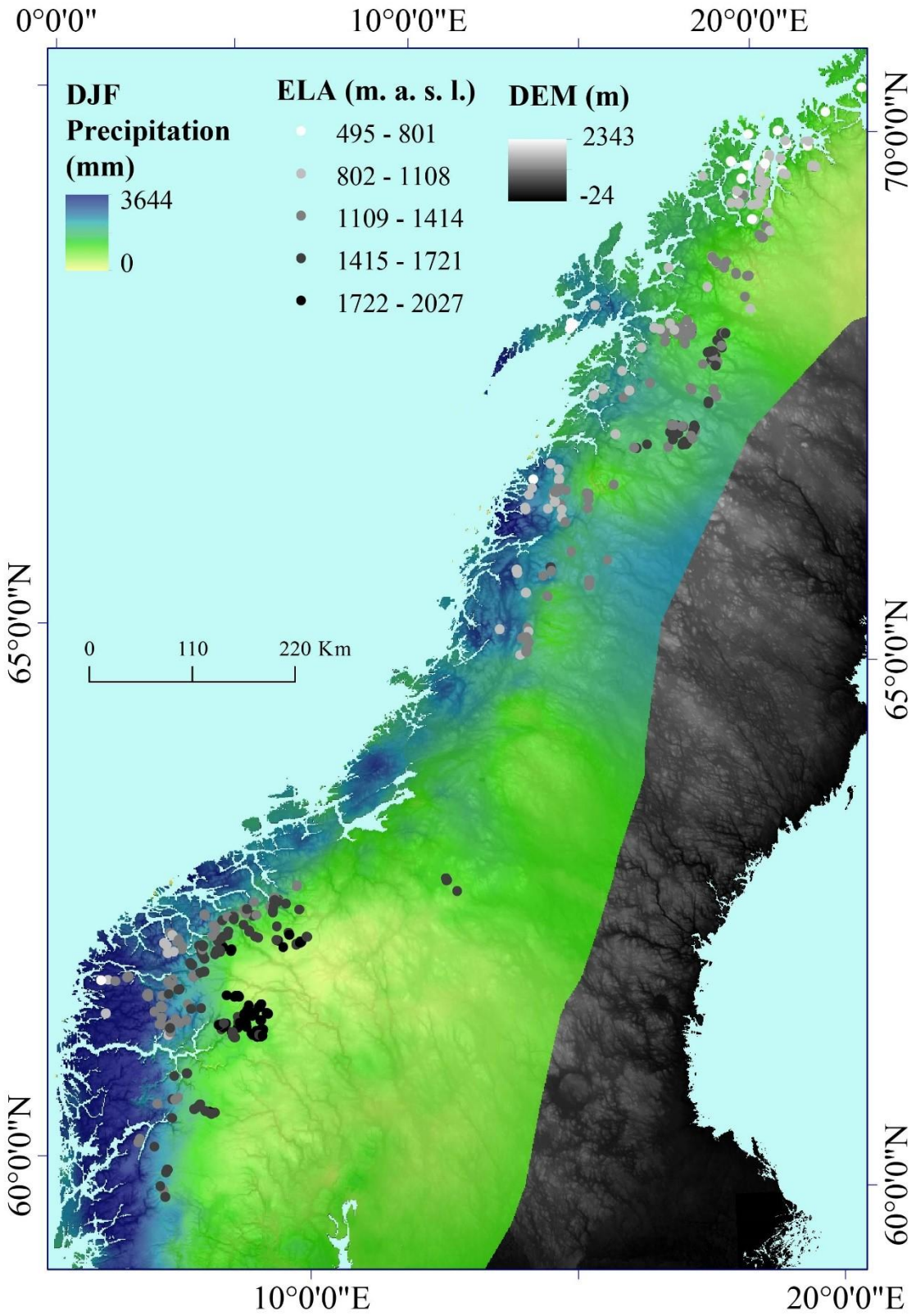


365  
366 Figure 2: Example of two cirque glaciers analysed in this study. (a) Cirque glacier polygons obtained  
367 from the NVE. Also shown are 15 m elevation contours derived from the NVE DEM. (b) The same  
368 area viewed in a Google Earth image from the end of the ablation season in 2006, used to verify the  
369 presence of these glaciers. The top glacier is GLIMS ID G009186E62298N and the bottom glacier is  
370 GLIMS ID G009194E62289N location near the mountain Storstygesvånåtinden.



371

372 Figure 3: Present day (1976-2006) mean summer temperature (JJA) across the study area. Modern  
 373 cirque glacier ELAs are also shown. Climate data and DEM were obtained from the NVE.



376 Figure 4:

377 Present day (1976-2006) winter precipitation across the study area. Modern cirque glacier ELAs are  
 378 also shown. Climate data and DEM were obtained from the NVE.

	Solar Radiation	Latitude	Annual Precipitation	Winter Precipitation	Mean Annual Temperature	Distance to Coast	Mean Summer Temperature	Longitude
ELA (total)	0.347	-0.684	-0.187	-0.249	-0.667	0.817	-0.828	-0.585
North	0.159	-0.505	0.118	0.105	-0.853	0.788	-0.650	-0.224
South	0.277	-0.165	-0.783	-0.790	-0.878	0.741	-0.806	0.545

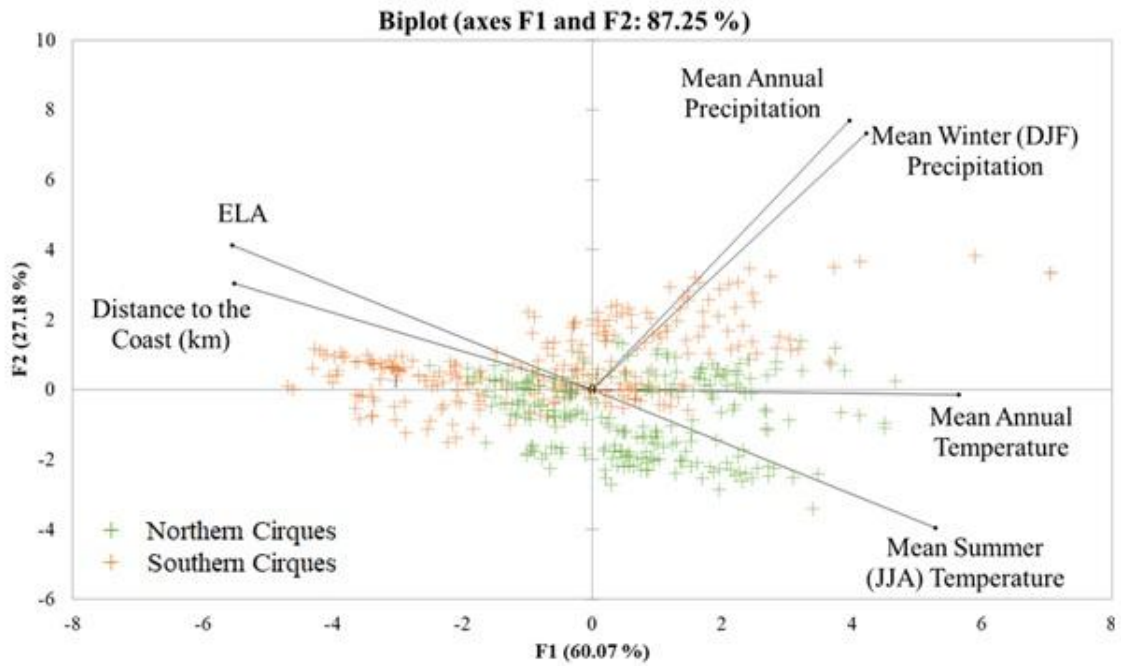
379

380 Table 1: Pearson correlations between ELA and topographic and climatic variables (at the ELA). All  
 381 variables are statistically significant to 0.05. Dark grey shading represents ‘very strong correlations, ±  
 382 0.75 - 1.0; medium grey ‘strong’ correlations, ± 0.5 - 0.749; light grey ‘weak’ correlations ± 0.25 -  
 383 0.499; and white ‘very weak’ correlations, ± 0.0 - 0.249.

	Latitude	Annual Precipitation	Winter Precipitation	Mean Annual Temperature	Distance to Coast	Mean Summer Temperature	Longitude
<b>Distance to Coast (total)</b>	-0.568	-0.266	-0.311	-0.668	-	-0.697	-0.414
North	-0.337	-0.142	-0.107	-0.843	-	-0.431	0.052
South	-0.514	-0.558	-0.582	-0.763	-	-0.643	0.445

384

385 Table 2: Pearson correlations between distance from the coast and other topographic and climatic  
 386 variables at the cirque glacier ELA. All variables are statistically significant to 0.05. Shading to  
 387 highlight correlation strength as for Table 1.

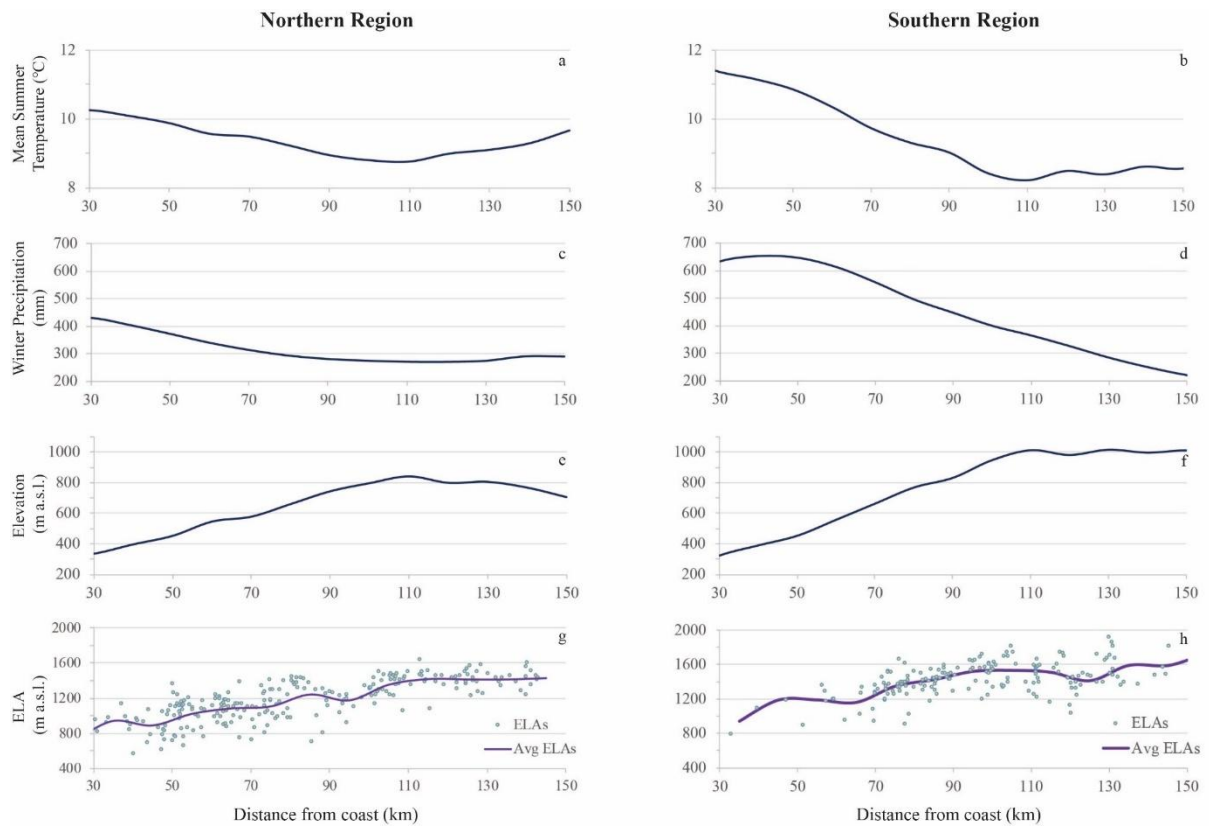


389

390 Figure 5: PCA of potential controls on Scandinavian cirque glacier ELAs. The orange crosses are the  
391 southern cirque glaciers and the green are the northern cirque glaciers. Northern cirque glaciers are  
392 distributed along the temperature component. Southern cirque glaciers are distributed along two  
393 components, precipitation and distance to coast, both reflecting the effect of continentality on  
394 southern cirque glacier distributions.

395

396



397

398

399

400

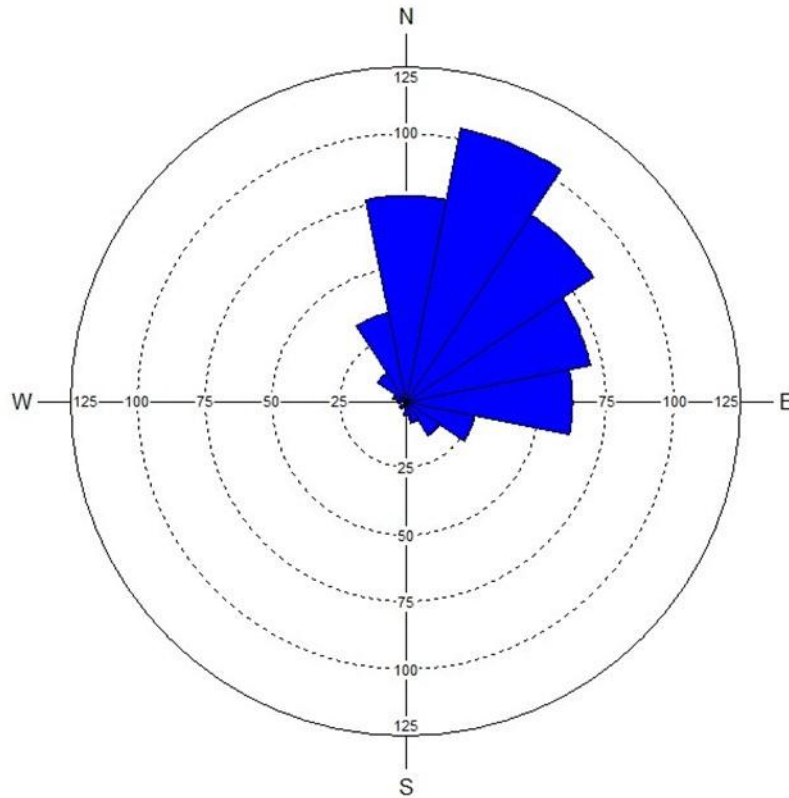
401

402

403

404

Figure 6: The plots show various trends with distance from the coast extracted within 10-km wide swaths that were generated parallel to the coast in both the south and north Scandinavia macro-regions: (a) mean summer air temperature in the northern region; (b) mean summer air temperature in the southern region; (c) winter precipitation in the northern region; (d) winter precipitation in the southern region; (e) mean topography in the northern region; (f) mean topography in the southern region; (g) average ELA in the northern region overlain with individual cirque glacier ELAs (blue dots); and (h) mean ELA in the southern region with individual cirque glacier ELAs.



405

406 Figure 7: Rose diagram of cirque glacier mean aspect (n = 513). Each bin is  $22.5^\circ$ , (i.e. North spans  
 407  $348.75 - 11.25$ ) and the radius is the quantity of cirque glaciers that fall within that aspect bin. The  
 408 mean direction of all cirque glacier aspects is  $41^\circ$ .

409

410 **8.0 References**

411 Anders, A. M., Mitchell, S. G. & Tomkin, J. H. Cirques, peaks, and precipitation patterns  
 412 in the Swiss Alps: Connections among climate, glacial erosion, and topography. *Geology*  
 413 **38**, 239–242 (2010).

414 Andreassen, L. M., Winsvold, S. H., Paul, F. & Hausberg, J. E. *Inventory of Norwegian*  
 415 *glaciers. NVE Rapport* **38**, (2012).

416 Baker, P. A. Paleo-Precipitation Indicators. in *Encyclopedian of Earth Science Series:*  
 417 *Encyclopedia of paleoclimatology and ancient environments* (ed. Gornitz, V.) **47**, 746–  
 418 748 (2009).

- 419 Bakke, J., Trachsel, M., Kvisvik, B. C., Nesje, A., & Lyså, A. (2013). Numerical analyses  
420 of a multi-proxy data set from a distal glacier-fed lake, Sørsendalsvatn, western Norway.  
421 *Quaternary Science Reviews*. <https://doi.org/10.1016/j.quascirev.2013.05.003>
- 422 Barr, I. D. *et al.* Climate patterns during former periods of mountain glaciation in Britain  
423 and Ireland: Inferences from the cirque record. *Palaeogeogr. Palaeoclimatol. Palaeoecol.*  
424 **485**, 466–475 (2017).
- 425 Barr, I. D. & Spagnolo, M. Understanding controls on cirque floor altitudes: Insights from  
426 Kamchatka. *Geomorphology* **248**, 1–13 (2015a).
- 427 Barr, I. D. & Spagnolo, M. Glacial cirques as palaeoenvironmental indicators: Their  
428 potential and limitations. *Earth-Science Rev.* **151**, 48–78 (2015b).
- 429 Benn, Douglas I.; Lehmkuhl, F. Mass balance and equilibrium-line altitudes of glaciers in  
430 high-mountain environments. *Quat. Int.* **65/66**, 15–29 (2000).
- 431 Braithwaite, R. J. Can the mass balance of a glacier be estimated from its equilibrium-line  
432 altitude? *J. Glaciol.* **30**, 364–368 (1984).
- 433 Braithwaite, R. J. & Raper, S. C. B. Estimating equilibrium-line altitude (ELA) from  
434 glacier inventory data. *Ann. Glaciol.* **50**, 127–132 (2009).
- 435 Carrivick, J. L. & Brewer, T. R. Improving Local Estimations and Regional Trends of  
436 Glacier Equilibrium Line Altitudes. *Geogr. Ann. Ser. A Phys. Geogr.* **86**, 67–79 (2004).
- 437 Chueca, J. & Julián, A. Relationship between solar radiation and the development and  
438 morphology of small cirque glaciers (Maladeta Mountain massif, Central Pyrenees,  
439 Spain). *Geogr. Ann. Ser. A Phys. Geogr.* **86**, 81–89 (2004).
- 440 Engelhardt, M., Schuler, T. V. & Andreassen, L. M. Evaluation of gridded precipitation  
441 for Norway using glacier mass-balance measurements. *Geogr. Ann. Ser. A Phys. Geogr.*  
442 **94**, 501–509 (2012).
- 443 Evans, I. S. Glacier distribution and direction in Svalbard, Axel Heiberg Island and  
444 throughout the Arctic: General northward tendencies. *Polish Polar Res.* **32**, 199–238  
445 (2011).
- 446 Evans, I. S. Local aspect asymmetry of mountain glaciation: A global survey of  
447 consistency of favoured directions for glacier numbers and altitudes. *Geomorphology* **73**,  
448 166–184 (2006a).
- 449 Evans, I. S. Glacier Distribution in the Alps : Statistical Modelling of Altitude and  
450 Aspect. *Geogr. Ann. Ser. A Phys. Geogr.* **88 A**, 115–133 (2006b).
- 451 Evans, I. S. & Cox, N. Geomorphometry and the Operational Definition of Cirques. *R.*  
452 *Geogr. Soc. (with Inst. Br. Geogr.* **6**, 150–153 (1974).



453 Fujita, K. Effect of precipitation seasonality on climatic sensitivity of glacier mass  
454 balance. *Earth Planet. Sci. Lett.* **276**, 14–19 (2008).

455 GLIMS and NSIDC. Global Land Ice Measurements from Space glacier database.  
456 Compiled and made available by the international GLIMS community and the National  
457 Snow and Ice Data Center, Boulder CO, U.S.A. (2005, updated 2018).

458 Grudd, H. Small glaciers as sensitive indicators of climatic fluctuations. *Geogr. Ann. Ser.*  
459 *A* **72 A**, 119–123 (1990).

460 Hanssen-Bauer, I. Regional temperature and precipitation series for Norway: Analyses of  
461 time-series updated to 2004. *Report* (2005).

462 Hertzberg, J. E., Schmidt, M. W. & Sciences, A. Encyclopedia of Geochemistry.  
463 *Elements* **15**, 137–138 (2019).

464 Ipsen, H. A., Principato, S. M., Grube, R. E. & Lee, J. F. Spatial analysis of cirques from  
465 three regions of Iceland: implications for cirque formation and palaeoclimate. *Boreas* **47**,  
466 565–576 (2018).

467 Jansen, H. L., Simonsen, J. R., Dahl, S. O., Bakke, J., & Nielsen, P. R. (2016). Holocene  
468 glacier and climate fluctuations of the maritime ice cap Høgtuvbreen, northern Norway.  
469 *The Holocene*, 26(5)(736\*755). <https://doi.org/10.1177/0959683615618265>

470 Kellogg, T. B. (1977). Paleoclimatology and paleo-oceanography of the Norwegian and  
471 Greenland Seas: The last 450,000 years. *Marine Micropaleontology*, 2(C), 235–249.  
472 [https://doi.org/10.1016/0377-8398\(77\)90013-5](https://doi.org/10.1016/0377-8398(77)90013-5)

473 Kjøllmoen, Bjarne (Ed.); Andreassen, Liss M.; Elvehoy, Hallgeir; Jackson, Miriam;  
474 Kjøllmoen, Bjarne; Melvold, K. *Glaciological investigations in Norway 2016. Norwegian*  
475 *Water Resources and Energy Directorate* (Norwegian Water Resources and Energy  
476 Directorate, 2017).

477 Křížek, M. & Mida, P. The influence of aspect and altitude on the size, shape and spatial  
478 distribution of glacial cirques in the High Tatras (Slovakia, Poland). *Geomorphology* **198**,  
479 57–68 (2013).

480 Lauritzen, S.-E. (1995). High-Resolution Paleotemperature Proxy Record for the Last  
481 Interglaciation Based on Norwegian Speleothems. *Quaternary Research*, 43, 133–146.

482 Lussana, C., Tveito, O. E., Uboldi, F. & Cristian, L. *seNorge v2.0, Temperature An*  
483 *observational gridded dataset of temperature for Norway METreport Title Date seNorge*  
484 *v2.0: an observational gridded dataset of temper-ature for Norway. Norwegian*  
485 *Meteorological Institute* (2016).

486 Mangerud, J., Nstegaard, S. ", Sejrup, H.-P., & Haldorsen, S. (1981). A continuous  
487 Eemian-Early Weichselian sequence containing pollen and marine fossils at Fjpsanger,  
488 western Norwav. *Boreas*, 10, 137–208.

- 489 Nesje, A. (2009). Latest Pleistocene and Holocene alpine glacier fluctuations in  
490 Scandinavia. *Quaternary Science Reviews*, 28(21–22), 2119–2136.  
491 <https://doi.org/10.1016/j.quascirev.2008.12.016>
- 492 Nesje, A. Topographical Effects on the Equilibrium Line Altitude on Glaciers.  
493 *GeoJournal* **27**, 383–391 (1992).
- 494 Nesje, A., Bakke, J., Dahl, S. O., Lie, Ø., & Matthews, J. A. (2008). Norwegian mountain  
495 glaciers in the past, present and future. *Global and Planetary Change*, 60(1–2), 10–27.  
496 <https://doi.org/10.1016/j.gloplacha.2006.08.004>
- 497 Norwegian Mapping Authority. The Terrain Model WMS Service Provides Information  
498 on the Terrestrial Terrain Model (DTM 10).  
499 [https://www.kartverket.no/data/Laserskanning/\(2016\)](https://www.kartverket.no/data/Laserskanning/(2016)).
- 500 NVE. Norwegian Water Resources and Energy Directorate (NVE). Climate indicator  
501 products, <http://glacier.nve.no/viewer/CI/>, downloaded <2017.12.01>. (2017).
- 502 Oerlemans, J. & Hoogendoorn, N. C. Mass-balance gradients and climatic change. *J.*  
503 *Glaciol.* **35**, 399–405 (1989).
- 504 Ohmura, A. & Boettcher, M. Climate on the equilibrium line altitudes of glaciers:  
505 Theoretical background behind Ahlmann’s P/T diagram. *J. Glaciol.* **64**, 489–505 (2018).
- 506 Ohmura, A. ; Kasser, P. ; Funk, M. Climate at the equilibrium line of glaciers. *J. Glaciol.*  
507 **38**, 397–411 (1992).
- 508 Olsen, L., Sveian, H., Ottesen, D. and Rise, L. (2013) Quaternary glacial, interglacial and  
509 interstadial deposits of Norway and adjacent onshore and offshore areas. In Olsen, L.,  
510 Fredin, O. and Olesen, O. (eds.) *Quaternary Geology of Norway*, Geological Survey of  
511 Norway Special Publication, 13, pp. 79–144
- 512 Osmaston, H. (2005). Estimates of glacier equilibrium line altitudes by the Area ×  
513 Altitude, the Area × Altitude Balance Ratio and the Area × Altitude Balance Index  
514 methods and their validation. *Quaternary International*, 138–139, 22–31.  
515 <https://doi.org/10.1016/j.quaint.2005.02.004>
- 516 Pearce, D. M., Ely, J. C., Barr, I. D. & Boston, C. M. Section 3.4.9: Glacier  
517 Reconstruction. in *Geomorphological Techniques (Online Edition)* **9**, (British Society for  
518 Geomorphology, 2017).
- 519 Pellitero, R. *et al.* A GIS tool for automatic calculation of glacier equilibrium-line  
520 altitudes. *Comput. Geosci.* **82**, 55–62 (2015).
- 521 Raper, S. C. B. & Braithwaite, R. J. Glacier volume response time and its links to climate  
522 and topography based on a conceptual model of glacier hypsometry. *Cryosphere* **3**, 183–  
523 194 (2009).

- 524 Raup, B. *et al.* The GLIMS geospatial glacier database: A new tool for studying glacier  
525 change. *Glob. Planet. Change* **56**, 101–110 (2007).
- 526 Rea, B. R. Defining modern day Area-Altitude Balance Ratios (AABRs) and their use in  
527 glacier-climate reconstructions. *Quat. Sci. Rev.* **28**, 237–248 (2009).
- 528 Rosqvist, G. & Østrem, G. The Sensitivity of a Small Icecap to Climatic Fluctuations.  
529 *Geogr. Ann. Ser. A Phys. Geogr.* **71**, 99–103 (1989).
- 530 Rudberg, S. Glacial cirques in Scandinavia. *Nor. Geogr. Tidsskr. - Nor. J. Geogr.* **48**,  
531 179–197 (1994).
- 532 Rupper, S. & Roe, G. Glacier changes and regional climate: A mass and energy balance  
533 approach. *J. Clim.* **21**, 5384–5401 (2008).
- 534 Sagredo, E. A., Rupper, S. & Lowell, T. V. Sensitivities of the equilibrium line altitude to  
535 temperature and precipitation changes along the Andes. *Quat. Res. (United States)* **81**,  
536 355–366 (2014).
- 537 Skoglund, R. Ø., & Lauritzen, S.-E. (2010). Morphology and speleogenesis of Okshola,  
538 Fauske, northern Norway: example of a multi-stage network cave in a glacial landscape.  
539 In *Norwegian Journal of Geology* (Vol. 90). Spagnolo, M. *et al.* ACME, a GIS tool for  
540 Automated Cirque Metric Extraction. *Geomorphology* **278**, 280–286 (2017).
- 541 Sutherland, D. G. Modern glacier characteristics as a basis for inferring former climates  
542 with particular reference to the Loch Lomond Stadial. *Quat. Sci. Rev.* **3**, 291–309 (1984).
- 543 Torsnes, I., Rye, N., & Nesje, A. (1993). Arctic and Alpine Research Modern and Little  
544 Ice Age Equilibrium-line Altitudes on Outlet Valley Glaciers from Jostedalbreen,  
545 Western Norway: An Evaluation of Different Approaches to their Calculation. *Arctic and  
546 Alpine Research*, 25(2), 106–116. <https://doi.org/10.1080/00040851.1993.12002990>
- 547 Trachsel, M. & Nesje, A. Modelling annual mass balances of eight Scandinavian glaciers  
548 using statistical models. *Cryosphere* **9**, 1401–1414 (2015).
- 549 Trenhaile, A. S. Cirque Morphometry in the Canadian Cordillera Author. *Ann. Association  
550 Am. Geogr.* **66**, 517–529 (1975).
- 551 Tveito, O. E. *et al.* DNMI - Nordic temperature maps. DNMI - Report **09/00 KLIM**,  
552 (Norwegian Meteorological Institute, 2000).
- 553 WGMS. Fluctuations of Glaciers Database. World Glacier Monitoring Service, Zurich,  
554 Switzerland. DOI:10.5904/wgms-fog-2018-11. Online  
555 access: <http://dx.doi.org/10.5904/wgms-fog-2018-11>. (2018).
- 556 WGMS, and National Snow and Ice Data Center (comps.). World Glacier Inventory,  
557 Version 1. Boulder, Colorado USA. NSIDC: National Snow and Ice Data Center. DOI:

- 558 <https://doi.org/10.7265/N5/NSIDC-WGI-2012-02>. [24 October 2018. (1999). updated  
559 2012.
- 560 Winkler, S., Elvehy, H. & Nesje, A. Glacier fluctuations of Jostedalsbreen, western  
561 Norway, during the past 20 years: The sensitive response of maritime mountain glaciers.  
562 *Holocene* **19**, 395–414 (2009).
- 563 Winkler, S. & Nesje, A. Perturbation of climatic response at maritime glaciers? *Erdkunde*  
564 **63**, 229–244 (2009).
- 565 Winsvold, S. H., Andreassen, L. M. & Kienholz, C. Glacier area and length changes in  
566 Norway from repeat inventories. *Cryosphere* **8**, 1885–1903 (2014).
- 567 Wong, W. K., Haddeland, I., Lawrence, D. & Beldring, S. Gridded 1 x 1 km climate and  
568 hydrological projections for Norway. 25 (2016).